

## Research Article

# Thin-Film Nanocomposite Membranes of Cellulose Nanocrystal/Silver (CNC/Ag) for Removal of Phenol Compounds

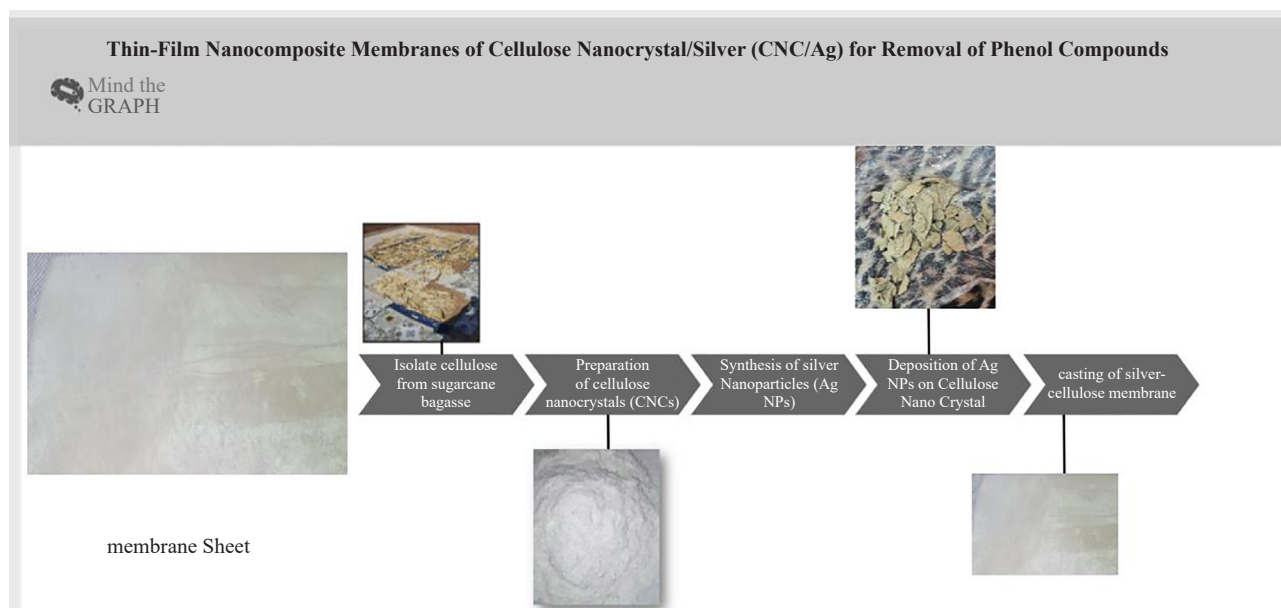
Samah A. Hawash<sup>1\*</sup>, Ahmed M. Enew<sup>1</sup>, Mahmoud H. Mahmoud<sup>2</sup>, Safaa R. Fouad<sup>1</sup>

<sup>1</sup>Chemical Engineering Department, Menoufia Higher Institute of Engineering and Technology-MNF-HIET, Menoufia, Egypt

<sup>2</sup>Mathematical and Physical Engineering Department, Faculty of Engineering, Mansoura University, El Mansoura, Egypt  
Email: samah.mohamed@bie.edu.eg.

Received: 11 June 2024; Revised: 5 August 2024; Accepted: 21 August 2024

## Graphical Abstract



**Abstract:** Bagasse is the sugar cane residue obtained from the sugar industry. It is produced in large quantities and used to make paper because of its fibrous structure. In the present research, sugarcane bagasse (SCB) was chemically treated with  $\text{HNO}_3$ ,  $\text{NaOH}$ , and a bleaching agent to recover 58% of the chemically purified cellulose (CPC), which was subsequently hydrolyzed with  $\text{H}_2\text{SO}_4$  to form cellulose nanocrystal (CNC). The capacity of a composite membrane made of cellulose nanocrystal (CNC) enhanced with silver nanoparticles (Ag NPs) to extract phenols from petrochemical effluent was examined. The prepared membrane was examined using a scanning electron microscope (SEM), transmission electron microscopy (TEM), and X-ray diffraction (XRD). The results showed that the white spot on the crystal surface suggested AgNP agglomeration on the CNC surface. The nanocellulose possessed crystallinity

Copyright ©2024 Samah A. Hawash, et al.  
DOI: <https://doi.org/10.37256/fce.5220245128>  
This is an open-access article distributed under a CC BY license  
(Creative Commons Attribution 4.0 International License)  
<https://creativecommons.org/licenses/by/4.0/>

indices ranging from 21.9 to 33.1 nm, whereas the silver particles measured 23 and 62 nm. The high separation result of phenol obtained at casting composition of 14% Ag NPs reached 60% at an equilibrium time of 45 min and pH 9. The isothermal and kinetic analysis explained that the rate of adsorption process is the pseudo-second order and followed the Freundlich isotherm models. The CNCs generated using this approach were found to be less agglomerated and more crystalline, indicating a better potential as bio-nanocomposite materials for wastewater treatment.

**Keywords:** bagasse, silver nanoparticles, cellulose nanofibers, phenol removal

## 1. Introduction

Oil drilling operations can create large quantities of contaminated water known as PW “Produced Water”, oilfield water, the naturally occurring water that comes out of the ground along with oil and gas. It is a mixture of different organic and inorganic compounds and its discharge can pollute soil and surface/underground water. The challenge to the oil industry is the adoption of technologies for the treatment of contaminated water that is economically feasible. The physical and chemical properties of PW vary considerably depending on the geographic location of the field, the geologic formation from where the water is produced, and the type of hydrocarbon product being produced.<sup>1</sup>

The common treatments for wastewater are ion exchange, adsorption, electrochemical, chemical deposition, and biotechnology. They include chemical, physical, and biological processes. Table 1 shows the selection of one of them depends on various factors such as sewage composition, salt and oil concentration, additional impurities present in wastewater, and processing cost. Each method has distinctive features that can be beneficial but restricted in another.<sup>2</sup>

**Table 1.** Phenol removal using different techniques

References	Techniques	Result	Disadvantages
Pillai et al. <sup>7</sup>	Adsorption and extraction methods	eliminate any phenol amount, whether at a trace level or a predetermined percent concentration	depending on the economics of using and recycling the required secondary material, adsorbent, or extractant
Saputera et al. <sup>8</sup>	Liquid-liquid extraction	suitable over a wide range of phenol concentrations (50-2,200 mg/L)	it is cost-effective in some circumstances
Dhali et al. <sup>9</sup>	Membrane technologies	reliable and economically feasible to treat phenol and have many advantages such as low power consumption, high quality effluent, small footprint, and easy scaling up with membrane modules	consideration must be given to membrane fouling which can occur due to particles and colloids present in the feed streams

Recent advances in nanotechnology have provided the scope and opportunities to fabricate sustainable nanomaterials that are more efficient, functional, and environmentally friendly than their parent materials. A typical mixed-matrix membrane contains a dispersion of nanoparticles in a bulk continuous polymer phase inheriting some of the characteristics of inorganic particles, especially their superior separation performance.<sup>3</sup>

A naturally occurring polymer produced from agricultural waste has become an increasing concern in recent years. Cotton, banana rachis, corncob, rice husk, and sugarcane bagasse are among the materials that can be used to make cellulose. As a result, a top contender is taken into account when creating sustainable adsorbent platforms for use in water remediation. Cellulosic materials, both natural and artificial, are utilized to filter out organic and inorganic contaminants from wastewater.<sup>4</sup> Several review articles have been published on cellulose-based inorganics. Ahmed Salama studied the driving forces and limitations of structuring cellulose/calcium phosphate hybrid materials.<sup>5</sup> The use of cellulose as an alternative to synthetic polymers might permit the decrease of environmental impacts by achieving more easily biodegradable or reusable materials. Recently, cellulose and inorganics have been synergistically coupled to tailor promising functional hybrids with unique properties such as cellulose/calcium phosphate composites. However, Hanif et al. implemented strategies that involve synthesis by multi-step and utilize environment-non-friendly reducing

agents for the deposition of Ag NPs on CNCs.<sup>6</sup> Furthermore, the long-time aqueous dispersion stability of prepared Ag NPs hybrids is another issue of concern for their efficient utilization as an antibacterial filler.

This work aims to separate cellulose from sugarcane bagasse and create a membrane sheet from a composite of CNF and Ag NPs to remove phenol from oil refining company wastewater.

## 2. Materials and methods

### 2.1 Raw materials

Sugar cane bagasse was obtained from cane juice warehouses and subsequently processed to make it suitable for usage. The material specifications and suppliers are given in Table 2.

**Table 2.** Specifications, and supplier of the raw materials used in membrane preparation

Material	Specification	Supplier
Acetic acid	Molar mass: 60.052 g/mol Density: 1.05 g/cm <sup>3</sup>	Alpha Chemika
Sodium hypochlorite	Molar mass: 74.44 g/mol Density: 1.11 g/cm <sup>3</sup>	Al, Jumhuria's Cairo Chemical Co.
Acetone	Molar mass: 58.08 g/mol Assay: 99%	Al, Jumhuria's Cairo Chemical Co.
Nitric acid	Molar mass: 63.01 g/mol Density: 1.51 g/cm <sup>3</sup> Assay: 68%	Al, Jumhuria's Cairo Chemical Co.
Sulfuric acid	Molar mass: 98.079 g/mol Density: 1.83 g/cm <sup>3</sup> Assay : 80%	Al, Jumhuria's Cairo Chemical Co.
Sodium Hydroxide	Molar mass: 39.997 g/mol	Al, Jumhuria's Cairo Chemical Co.
Silver Nitrate	Molar mass: 169.87 g/mol	Al, Jumhuria's Cairo Chemical Co.
Ammonia solution	Molar mass: 35.04 g/mol Density: 880 kg/m <sup>3</sup>	Al, Jumhuria's Cairo Chemical Co.
Cetyltrimethylammonium bromide (CTAB)	Molar mass: 364.45 g/mol	Al, Jumhuria's Cairo Chemical Co.
Sodium borohydride (NaBH <sub>4</sub> )	Molar mass: 37.83 g/mol	Al, Jumhuria's Cairo Chemical Co.

### 2.2 Methods

#### 2.2.1 Preparation of sugarcane bagasse

Sugarcane bagasse was cleaned using distilled water, as shown in Figure 1. Then it was sun-dried for 24 hours, oven-dried for approximately one and a half hours at 80 °C, and finally kept at room temperature at the lab.



**Figure 1.** Drying steps of bagasse

### 2.2.2 Isolation process

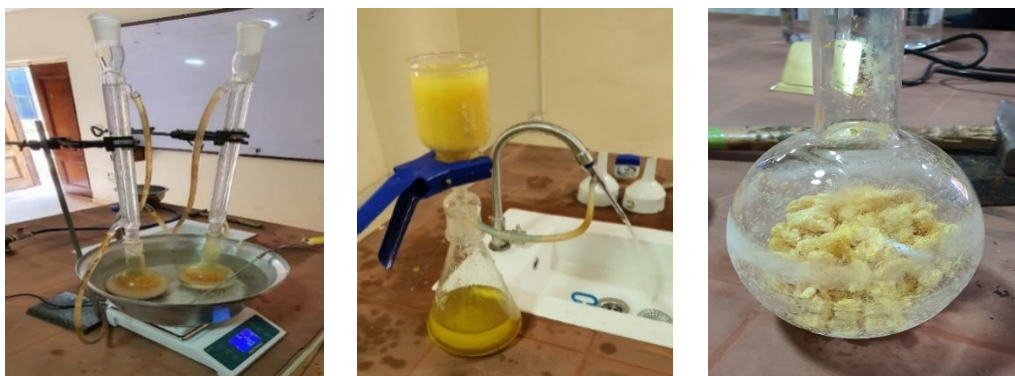


**Figure 2.** Hydrolysis of sugarcane bagasse with  $\text{HNO}_3$

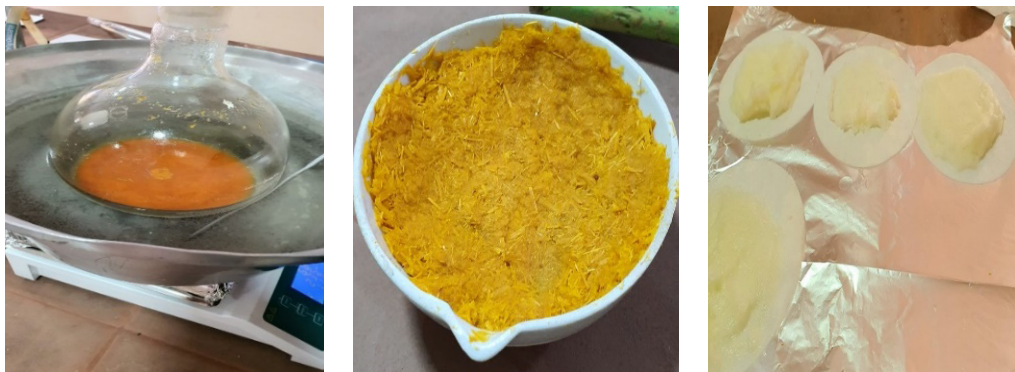


**Figure 3.** Neutralizing and bleaching of cellulose

The stages of cellulose isolated from sugarcane bagasse are depicted in Figures 2 to 3. After two hours in a hot water bath at  $80\text{ }^\circ\text{C}$ , 70 g of bagasse powder and 700 mL of 6% (w/v)  $\text{HNO}_3$  were combined. The mixture was then neutralized with deionized water. After that, the solution was refluxed for two hours at  $80\text{ }^\circ\text{C}$  in a hot water bath using 500 mL of 1%  $\text{NaOH}$  while being constantly stirred. Deionized water was used for washing, and 250 mL of sodium hypochlorite 0.735% (w/v) was used for bleaching. The lignocellulosic extract was mixed with acetic acid and heated to  $80\text{ }^\circ\text{C}$  for two hours. After being cleaned with deionized water to a pH of neutral, the residue was allowed to dry for three days at room temperature. This step was done by nitric acid ( $\text{HNO}_3$ ) to reduce the hemicellulose to about (3-5%)

and (1.6%) lignin, then followed by sodium hydroxide to reduce it even more (3%) of hemicellulose and (0.3%) of lignin. The recovery of cellulose from this step was 58%.<sup>10</sup>

### 2.2.3 Preparation of cellulose nanocrystals (CNCs)

The process of hydrolyzing SCB with 32% (w/v) of  $\text{H}_2\text{SO}_4$  at a ratio of 1:25, at room temperature for 24 hours, while being continuously agitated, produced chemically purified cellulose (CPC). Centrifuging the mixture three times for fifteen minutes at 10,000 rpm was used to extract the acidic solution after adding ten times as much deionized water to quench the reaction. After the sediment was removed, the cellulose precipitate was once again distributed in deionized water and repeatedly dialyzed against deionized water. Figure 4 illustrates how the colloidal solution was sonicated for an hour in an ice bath sonicator. Following a 24-hour rest period, acetone was added in place of the water, and the mixture was centrifuged for 30 minutes at 6,000 rpm. Ultimately, the nanoparticles of cellulose were oven-dried overnight at 70 °C in a vacuum.<sup>11</sup>



Figure 4. Preparation steps of cellulose nanocrystals

### 2.2.4 Synthesis of silver nanoparticles

As a stabilizing agent, 0.009 g of ( $5 \times 10^{-4}$  M) CTAB (0.009 of CTAB diluted in 10 ml distilled water) and 0.009 g of ( $2 \times 10^{-3}$  M)  $\text{AgNO}_3$  solution were used, respectively, in the synthesis of silver nanoparticles. To bring the solution to an alkaline medium, ammonia solution (0.04 M) was added. The solution combination rapidly stirred as it cooled in an ice bath for 30 minutes. To create silver colloidal dispersion, 25 ml of an  $8 \times 10^{-3}$  M aqueous solution of  $\text{NaBH}_4$  was added and aggressively stirred in an ice bath for 4 hours.<sup>12</sup> After adding the requisite amount of ammonia, the translucent, colorless reaction mixture containing  $\text{AgNO}_3 + \text{CTAB}$  took on the distinctive pale-yellow hue. It noted that color appeared. The appearance of silver nanoparticles was indicated by the formation of color, and the silver ion was analyzed using a UV-spectrophotometer with a wavelength of 409 nm.

### 2.2.5 Deposition of Ag NPs on cellulose nanocrystal

A different molar concentration of Ag nanoparticles ranging from 0.5, 1, and 2 molar was prepared and put into three beakers. 50 ml of pure water and 10 gm of CNC were mixed, and the mixture was then gently put into each beaker. The samples were taken out of the beaker and thoroughly rinsed with water to get rid of any loosely bound Ag NPs after being stirred for 24 hours. The composite was subsequently air-dried before being placed in each Petri dish for additional examination.<sup>13</sup>

### 2.2.6 Immersion casting of silver-cellulose membrane

One of the most popular techniques for creating polymeric membranes is immersion casting. In this method, which is called the non-solvent-induced phase separation (NIPS) technology, the cast film, which is composed of Ag-



Nano-cellulose and PVC, is immersed in a coagulation bath that contains a nonsolvent, where the phase separation process takes place. The most common nonsolvent is often water, although you may also use pure organic solvents like 1-methyl-2-pyrrolidinone or other aqueous solutions. The exchange of solvent and nonsolvent in the cast film determines membrane development by polymer precipitation. Following immersion, the cast film splits into two phases: a solvent-rich phase forms the membrane's pores, and a polymer-rich phase forms the membrane matrix. The various membrane structures are caused by variations in the polymer concentration (PVC).<sup>14</sup> The membrane is prepared by adding 20 g of 1-methyl-2-pyrrolidinone to a silver-nano cellulose nanocomposite and PVC mass ratio. To get a homogeneous suspension, the mixture was sonicated for 10 minutes and then swirled for an additional 30 minutes. After a few seconds, the prepared solution expanded onto the glass surface and was submerged in cool water to separate the membrane from the glass surface.

### 2.2.7 Equilibrium studies of adsorption of phenol on CNC-Ag NPs composites

The effects of several variables, including contact time, pH, and the concentration of silver nanoparticles, modified the surface of the membrane and were investigated in batch adsorption techniques using 100 mL of wastewater collected from Cairo Petroleum Refining Company "CORC-Tanta" with a phenol concentration of 0.1 mg/l, pH 7, and at a temperature of 20 °C was employed. At varying contact times of 15, 30, 45, 60, 90, and 120 min, samples were filtered and allowed to pass through the membrane sheet. The samples were examined in a UV spectrophotometer at 292 nm wavelength after filtration to calculate the equilibrium contact time and measure the percentage of phenol removed.

### 2.2.8 Characterization

#### 2.2.8.1 X-ray diffraction analysis (XRD)

XRD determines the crystallinity of the following various treatment phases. Samples that had been freeze-dried were compacted into discs 10 mm in diameter. At an operational voltage and current of 40 kV and 40 mA, respectively, XRD of the samples were obtained and the following Eq. (1)<sup>15</sup> was used to calculate the Segal crystallinity index (*CrI*).

$$CrI = \frac{I_{002} - I_{am}}{I_{002}} \times 100\% \quad (1)$$

Where;

$I_{002}$ : The intensity of the highest intensity peak at 22.5°,

$I_{am}$ : The intensity of the amorphous peak at 18°, and

*CrI*: The relative degree of crystallinity.

#### 2.2.8.2 Transmission electron microscopy (TEM)

Using a transmission electron microscope, the morphological properties and particle sizes of the CNC-Ag NPs were assessed. The samples were placed on a copper grid that had been coated with carbon after being spread out in a suitable medium. The samples were then dried and TEM inspection was performed at an accelerating voltage of approximately 100-120 kV. The Image-Pro Plus application might be used to determine the CNCs' diameter spread.

#### 2.2.8.3 Scanning electron microscope (SEM)

Field emission SEM analysis was performed on samples following various treatment phases. Following various treatment phases, several nanocrystal surface morphologies were noted.

### 3. Results and discussion

#### 3.1 Scanning electron microscopy (SEM)

The synthesized particles have an uneven surface and a flaky structure, as seen in Figure 5. The composites were sonicated for 10 min and stirred for another 30 min until a homogenous suspension was obtained. White spots on the crystal surface are evidence of the deposition of Ag NPs.<sup>16</sup>

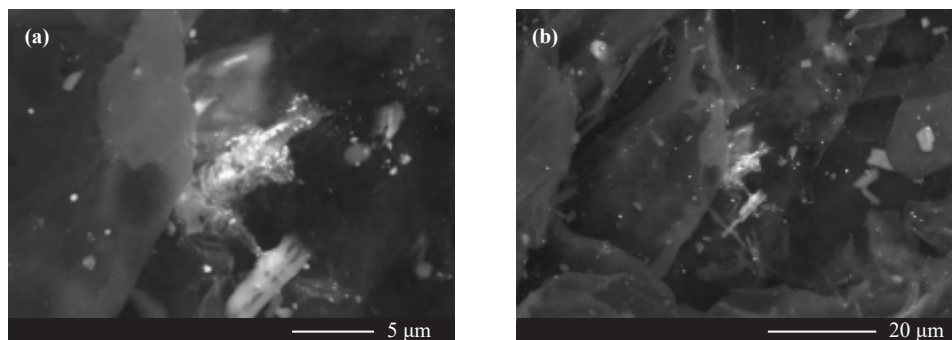


**Figure 5.** SEM images show the white spot of Ag NPs on the surface of CNC-Ag NPs composites, (a) 15,000x, (b) 5,000x

#### 3.2 Transmission electron microscopy (TEM)

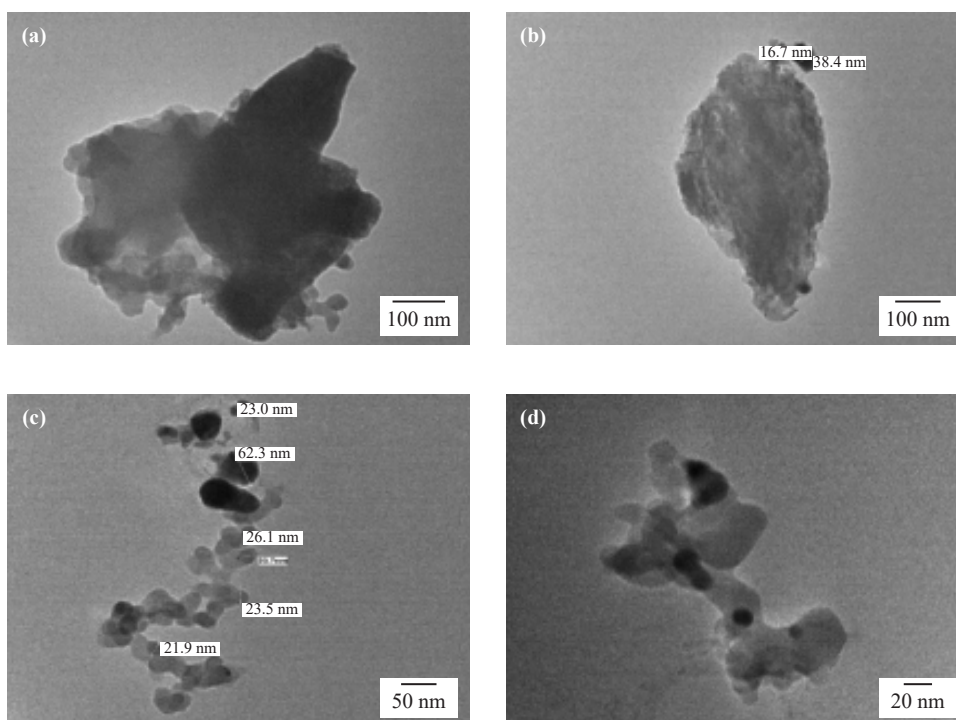


**Figure 6.** TEM images show the black Ag NPs on the surface of CNC-Ag NPs composites using different scales, (a) & (b) 100 nm, (c) 50 nm, (d) 20 nm

The morphology of Ag NP and CNC particle sizes were determined using TEM images. The removal of hemicellulose and lignin, which are components of the amorphous area of cellulose bagasse, is ensured by reducing the size of the cellulosic nanomaterials. The cross-section of CNCs varied from 21.9 to 33.1 nm, as shown in Figure 6. At the border of CNC crystals, a thin black line of Ag NP was visible. The TEM picture shows that several thick darks cover several Ag NP layers; the size of each Ag NP was found to be between 23 and 62 nm. Comparing this study to others, it is evident that the particles are more spherical in form and exhibit less aggregation. The surface ionic charge that caused the crystallites to stack together as a result of the acid hydrolysis process is responsible for this agglomeration.<sup>17</sup>

### 3.3 X-ray diffraction (XRD)

Three main components make up most natural plant fiber: cellulose, hemicellulose, and lignin. In their natural state, lignin and hemicellulose are amorphous. Because of hydrogen bonds and van der Waals forces in its molecular chain, cellulose easily crystallizes. Thus, alterations in the content and structure of the fiber are reflected in variations in the crystallinity of cellulose fibers. To determine which crystalline phases were present in the CNCs, XRD studies were looked at. The study displays the distinctive peaks of the solid components seen in CNCs. The sizes and crystallinity indices of samples taken at different treatment phases are displayed in Table 3 and Figure 7. 72% of CNCs had crystallinity indices. Because non-cellulosic components were gradually eliminated at each treatment step, the fiber's crystallinity index rose. The peaks stand in for the distinctive cellulose polymorph patterns. Ag nanoparticles were present in the clean CNC-Ag NPs composites, as shown by the XRD study, which had peaks at  $2\theta = 38.076^\circ$ ,  $44.412^\circ$ ,  $64.408^\circ$ , and  $77.259^\circ$ .<sup>18</sup>

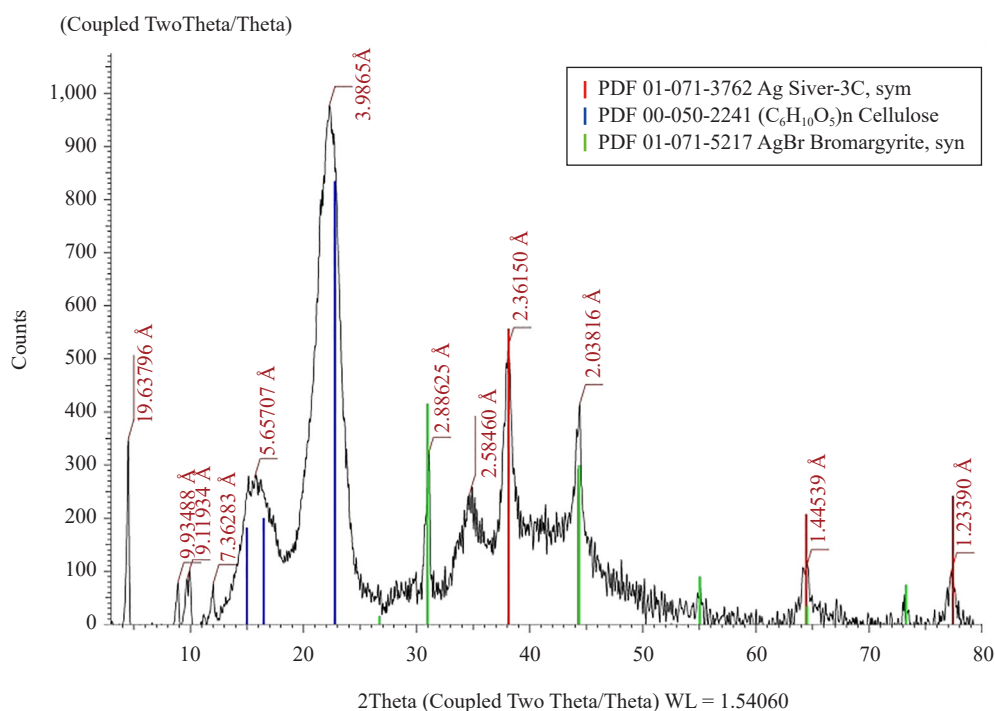








Figure 7. X-ray diffraction patterns of CNC-Ag NPs composites

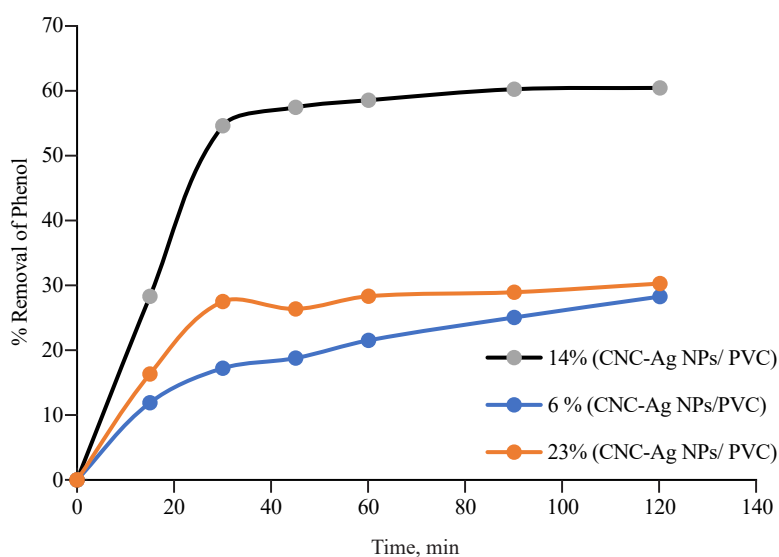


**Table 3.** Crystallite size of CNC-Ag NPs composites

Visible	Icon	Color	Index	Compound Name	Formula	S-Q
Yes			1	Silver-3C, syn	Ag	3.6%
Yes			2	Cellulose	C <sub>6</sub> H <sub>10</sub> O <sub>5</sub>	92.2%
Yes			3	Bromargyrite, syn	AgBr	4.2%

### 3.4 The effect of casting composition

The CNC-Ag NP composites to PVC mass percent is one of the most influencing factors in producing membranes with uniform pores. Because PVC has a minimal water flow and is hydrophobic, its use in membrane technology is constrained. By enhancing the hydrophilicity of the PVC membrane surface with hydrophilic additives and/or polymers, this restriction can be overcome.<sup>19</sup> Figure 8 shows the varying concentrations of CNC-Ag NPs Composites to PVC in the range of 6, 14, and 23 wt % at a temperature of 20 °C, pH 7, and concentration of 2 molar Ag NPs. The membrane means pore size and porosity improved as concentration increased up to 14wt% of (CNC-Ag NPs / PVC). However, an increase in the concentration of the casting solution caused a decrease in porosity due to particle agglomeration, and the dense film was obtained, decreasing the percent removal of phenol.<sup>20</sup>

**Figure 8.** Effect of casting composition on removal of phenol

### 3.5 The effect of equilibrium time & molar concentration of Ag NPs

Variations in the quantity of Ag NPs loading to nanocellulose were observed at pH 7, 20 °C, and 14% casting fixed concentration (CNC-Ag NPs /PVC). Figure 8 demonstrates how the proportion of phenol removed rose quickly in the first thirty minutes. After 45 minutes, the percentage of removal rose extremely slowly until stabilizing at 120 minutes. This indicates that after 45 minutes, the reaction achieved equilibrium and its maximum value. There was produced a strong driving force greater than the mass transfer resistance between the solid and aqueous phases. This was the cause of the initial rapid adsorption of phenol molecules, which subsequently reduced before reaching equilibrium.

Because of the repulsive interactions between the phenol molecules and the adsorbent surfaces, the unoccupied sites on the adsorbent could not be loaded with phenol molecules, allowing for the maximum phenol uptake to be reached at equilibrium.<sup>21</sup>

Additionally, Figure 9 showed that as the molar concentration of Ag NPS increased, the elimination of phenol increased from 45% to 60%. Sahoo et al. stated that the presence of Ag<sup>+</sup> nanoparticles coated in O-ions and cellulose-like structures with many hydroxyl groups in the CNC and Ag NPs of the composites.<sup>22</sup> There are three potential ways that phenol might attach itself to CNC-Ag NPs. One of the possible adsorption processes is the formation of hydrogen bonds between the phenol and CNC-Ag NPs composite molecules. This is because, according to Chinthalapudi et al.<sup>23</sup>, hydrogen bonds are formed between the hydroxyl section of CNC and the hydroxyl layer that surrounds charged Ag NPs and phenol molecules. The phenol molecules may stick to one another through the creation of a hydrogen bond.

Another possible adsorption process is the interaction of ions with dipoles. In the composites, the oxygen bonded to the hydroxyl group of the CNC will produce a negative dipole effect. Consequently, it is proposed that ion-dipole interaction may be the mechanism via which the positively charged phenol molecules and the oxygen atom on the hydroxyl group interact. This interaction of O<sup>-</sup> ions attached to Ag<sup>+</sup> nanoparticles in the composites can interact electrostatically as well, which might have contributed to the adsorption of phenol molecules onto the composites.<sup>24</sup>

Understanding the effect of pH on phenol removal will help in understanding the primary adsorption process between CNC-Ag NP composites and phenol molecules, even if this mechanism is currently unclear. pH variations have an impact on particles, and the ion-dipole interaction, and may even prevent hydrogen bonding. There could have been a greater contact between the composite and phenol molecules, though, because the composites were cured for a lengthy duration. The predominant adsorption mechanism behind the interaction between phenol molecules as the adsorbate and CNC-Ag NP composite as the adsorbent is thought to be physical adsorption caused by hydrogen bonding.

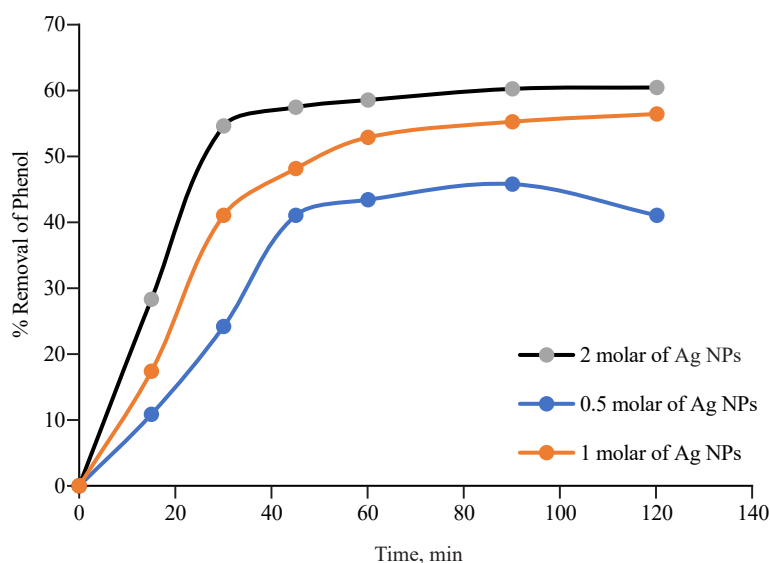
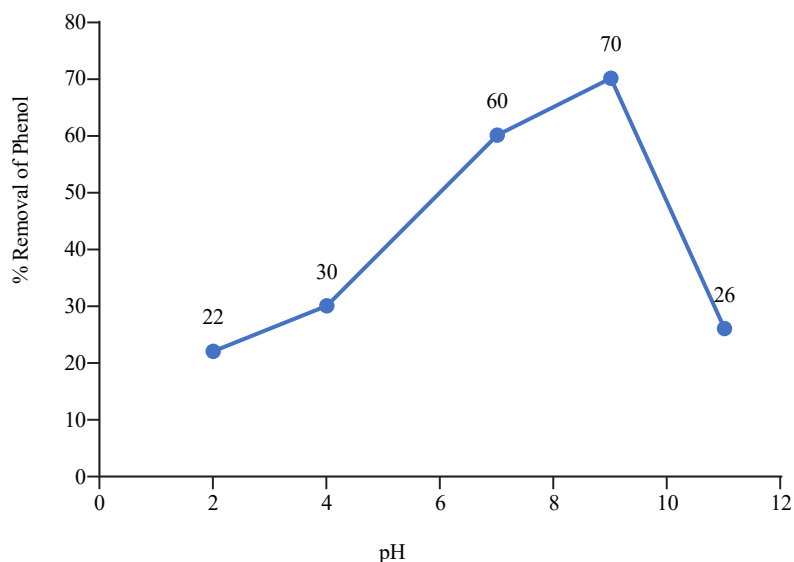


Figure 9. Effect of molar concentration of Ag NPs on removal of phenol

### 3.6 The effect of pH of the petroleum wastewater

According to Figure 10, removal efficiency improved from 20 to 70% when pH was raised from 2 to 9. However, as pH was raised further, removal efficiency was also seen to gradually decline, reaching 26% at pH 11. As a result, it was determined that pH 9 was ideal for phenol adsorption. Since phenol is a weak acid with a pKa of 9.89, it often dissociates at pH values higher than its pKa. When the pH of phenol in a solution is less than the phenol's pKa, the dominant species in the solution are the positively or neutrally charged phenol molecules. Therefore, at a pH lower than

the dissociation, maximal adsorption performance is seen. However, when the phenol's pH is greater than its pKa, the ionic form results from the aromatic ring being partly negatively charged due to the ionization of the hydroxyl group. Consequently, electrostatic interaction-which may be either repulsive or attractive-is the main mechanism. Therefore, electrostatic repulsion between negatively charged CNC and phenolate ions may be the cause of the observed increasing decline in adsorption performance.<sup>25</sup>



**Figure 10.** Effect of pH of petroleum wastewater on removal of phenol

### 3.7 Isotherms

To understand how the phenol molecules interact with the adsorbent and adhere to the surface, the adsorption process was investigated using Langmuir, Freundlich, and Temkin isotherms.

#### 3.7.1 Langmuir isotherm

The Langmuir isotherm characterizes the equilibrium connection between the phenol molecules adsorbed onto the adsorbent and adsorbate solution, as shown in Eq. (2). The fundamental presumption here is that there are no multilayers formed by the adsorbate and that every site is a flat plane devoid of any irregularities.

$$\frac{C_e}{q_e} = \frac{1}{bq_m} + \frac{1}{q_m}C_e \quad (2)$$

where  $b$  is the Langmuir isotherm constant (mg/l),  $q_e$  is the quantity of phenol adsorbed per unit mass of CNF-Ag NPs composite,  $q_m$  is the monolayer adsorption capacity (mg/g), and  $C_e$  is the phenol equilibrium concentration (mg/l).

$C_e/q_e$  and  $C_e$  were plotted using the effects of starting concentration and the experimental data, as seen in Figure 11. Additionally, the  $R^2$  values and the fitting equation are provided. These results suggested that the Langmuir adsorption isotherm was not well-fitted by the experimental data. These modifications made it possible to remove phenol using non-monolayer coverage. The likelihood and favorability of adsorption may be predicted using the equilibrium parameter ( $R_L$ ), a dimensionless constant. It is ascertainable as expressed in Eq. (3).

$$R_L = \frac{1}{1 + bC_0} \quad (3)$$

Eisa et al.<sup>26</sup> stated that adsorption is considered unfavorable if  $R_L > 1$  and linear if  $R_L = 1$ . The adsorption is considered linear if  $R_L = 1$ , favorable if  $0 < R_L < 1$ , and irreversible if  $R_L = 0$ . The present study's relative length ( $R_L$ ) was found to be between 0 and 1, indicating that the phenol adsorption using the CNF-Ag NPs composite is advantageous.

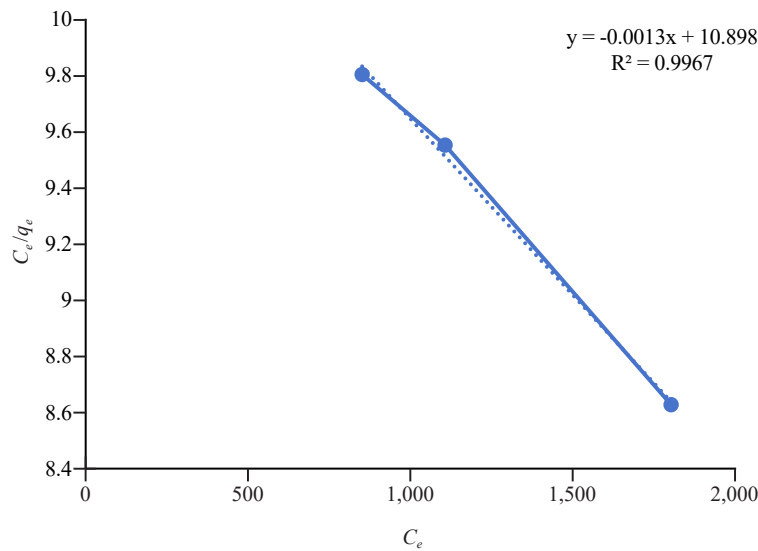


Figure 11. Linear plot of Langmuir isotherm

### 3.7.2 Freundlich isotherm

According to the Freundlich model, molecules that have been adsorbed on a heterogeneous surface interact and have a multilayer adsorption capacity. The Freundlich isotherm, which denotes multilayer adsorption, can be mathematically described as provided in Eq. (4).

$$q_e = K_f C_e^{1/n} \quad (4)$$

Where  $n$  is adsorption intensity and  $K_f$  is the Freundlich constant. Figure 12 shows a plot between  $\log(q_e)$  and  $\log(C_e)$ . Also provided are the  $R^2$  values and the fitting equation. The  $R^2$  value is calculated to be 0.9994, or nearly one. It implies that the physical multilayer adsorption of phenol on CNC-Ag NPs is the predominant process. Additionally, it shows that for modest concentrations, the Freundlich adsorption isotherm provides an excellent representation of the data.<sup>27</sup>

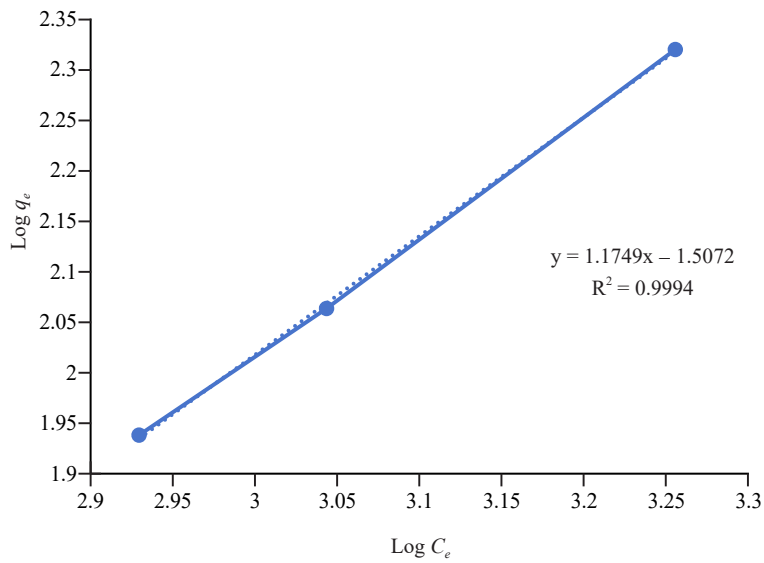


**Figure 12.** Linear plot of Freundlich isotherm

### 3.7.3 Temkin isotherm

The Temkin isotherm, as shown in Eq. (5), considers the effects of the indirect interactions between adsorbent and adsorbate molecules. For all surface molecules, it is found that the heat of adsorption decreases linearly with surface coverage.

$$q_e = \frac{RT}{b_T} \ln A_T + \frac{RT}{b_T} \ln C_e \quad (5)$$

where  $T$  is the temperature,  $R$  is the universal gas constant, and  $A_T$  and  $b_T$  are the fitting constants. The Temkin isotherm plot is shown in Figure 13. The computed  $R^2$  value is 0.9851

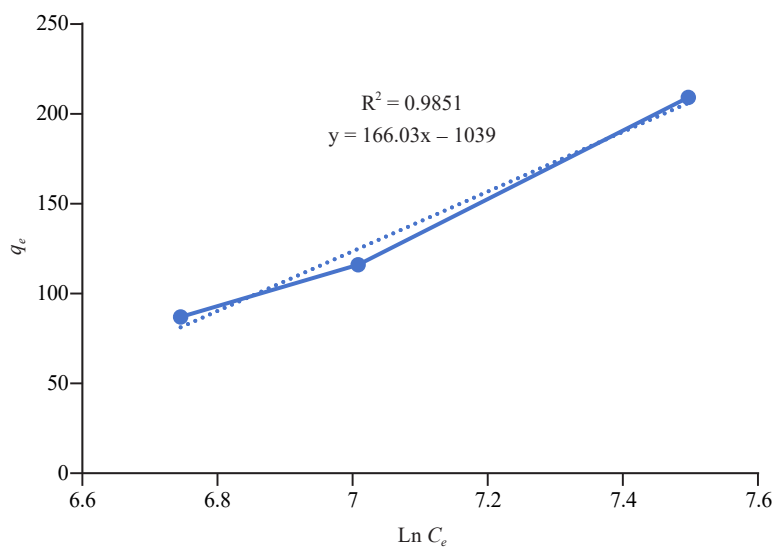


**Figure 13.** Linear plot of Temkin isotherm



The adsorption process matches the Freundlich isotherm, as can be shown from the  $R^2$  values of all isotherms.

### 3.8 Kinetics of adsorption

A dynamic model is used to represent the adsorption process route. Kinetic data are used to design adsorption systems and develop processes. There are four phases to the adsorption phenomenon. These are (i) the external adsorbent diffusing through the liquid film on the surface; (ii) the bulk adsorbent diffusing through a liquid film enclosing the solid adsorbent; (iii) the diffusion of the adsorbate, encompassing surface and pore diffusion; (iv) the interaction of physisorption or chemisorption with surface sites; The slowest step determines the total rate of adsorption.<sup>22</sup> The application of the first and second pseudo-order models allowed for a better understanding of the adsorption process.

#### 3.8.1 Pseudo-first order

The assumption behind the pseudo-first-order model is that the difference between saturation concentration and the rate at which solute uptake changes over time is directly proportional and represented by Eq. (6)

$$\log(q_e - q_t) = \log q_e - \left( \frac{k_1}{2.303} \right) t \quad (6)$$

Where  $k_1$  ( $\text{min}^{-1}$ ) is the rate constant. Figure 14 displays a  $\log(q_e - q_t)$  vs. time. The fitting equation and  $R^2$  values were calculated to be 0.9265

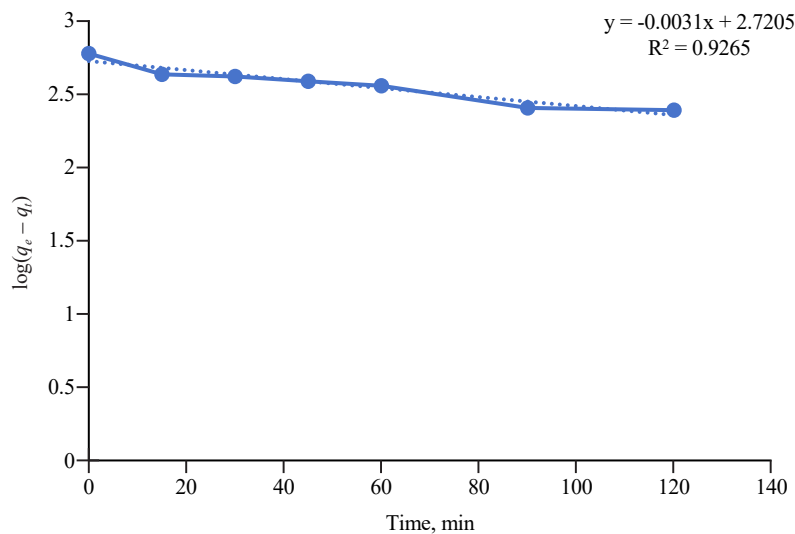


Figure 14. Linear plot of  $\log(q_e - q_t)$  versus time

#### 3.8.2 Pseudo-second order

According to the pseudo-second-order equation, the ratio of accessible active sites and its square root determines the adsorption rate, as shown in Eq. (7). Integrating this equation at initial conditions  $t = 0$  and  $q_t = 0$ , to become Eq. (8), where  $k_2$  is the pseudo-second-order isotherm's rate constant.

$$\frac{dq}{dt} = k_1 (q_e - q_t)^2 \quad (7)$$

$$\frac{t}{q_t} = \frac{1}{k_2 q_e^2} + \left(\frac{1}{q_e}\right)t \quad (8)$$

A plot of  $t/q_t$  vs time  $t$  (min) is presented in Figure 15.  $R^2$  was computed to have a value of 0.9819. A comparison of the pseudo-quadratic and pseudo-linear models is presented in Table 4. The pseudo-quadratic model ( $R^2 = 0.9819$ ) has a higher correlation value than the pseudo-first-order model ( $R^2 = 0.9265$ ). This implies that a better description of the adsorption process may be found in the pseudo-second-order kinetic model. The presence of active sites affects the adsorption kinetics, according to the interpretation of the data by a second-order pseudo-equation.<sup>28</sup>

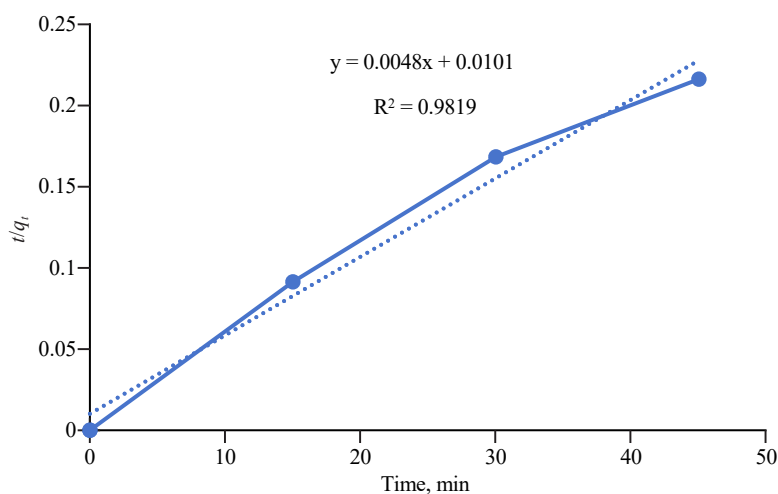


Figure 15. Linear plot of  $(t/q_t)$  versus time

Table 4. Kinetics model equation and rate constants

Order	Equation	Constant	$R^2$
Pseudo-linear order	$\log(q_e - q_t) = \log q_e - \left(\frac{k_1}{2.303}\right)t$	0.00714 min <sup>-1</sup>	0.9265
Pseudo-second order	$\frac{t}{q_t} = \frac{1}{k_2 q_e^2} + \left(\frac{1}{q_e}\right)t$	0.00228 g/(mg·min)	0.9819

## 4. Conclusion

The synthesis of cellulose nanocrystals (CNC) and the extraction of cellulose from sugarcane bagasse are supported by the research. The research investigated the effect of pH, optimum casting composition of silver nanoparticles on CNC and the equilibrium time required for the highest removal percent of phenol.

SEM images of the nanocrystals have a flaky structure with an uneven surface and revealed an increase in crystallinity, which pointed to the exposure of the crystalline phase following the effective removal of the lignin and hemicelluloses. While the CNC-Ag NPs composite's crystallinity indices and sample sizes obtained after different treatment phases are shown in XRD pictures.

The pore diameter of CNCs was measured by TEM to be between 21.9 and 33.1 nm, and the size of individual Ag NPs was found to be between 23 and 62 nm.

To create a membrane sheet with a consistent porosity of CNC-Ag NPs composite, the adsorption reaction reached equilibrium after 45 min. and the best casting composition is 14%.

Increase the % elimination of phenol by increasing the concentration of Ag NPs from 0.5 to 2 molar. The optimum pH was discovered to be 9, and phenol's adsorption efficiency dropped.

When CNF-Ag NPs composites were utilized and followed the Freundlich isotherm, multilayer physical adsorption was demonstrated by isotherm analysis. The kinetic investigations demonstrated that pseudo-second-order kinetics might provide a better description of the phenol adsorption on the CNF-Ag NPs composite powder.

## Conflict of interest

The authors declare no competing financial interest.

## References

- [1] Salama, A.; Hesemann, P. Recent trends in elaboration, processing, and derivatization of cellulosic materials using ionic liquids. *ACS Sustain. Chem. Eng.* **2020**, *8*, 17893-17907.
- [2] Salem, F.; Thiemann, T. Produced water from oil and gas exploration-problems, solutions, and opportunities. *J. Water Resource Prot.* **2022**, *14*, 142-185.
- [3] Patel, J.; Kumar, R. N.; Kumar, J. N. A comprehensive review on waste water treatment technologies with special emphasize on biological treatments. *Int. J. Life Sci. Pharma Res.* **2023**, *13*(2), L112-L124.
- [4] Wasim, M.; Mushtaq, M.; Khan, S. U.; Farooq, A.; Naeem, M. A.; Khan, M. R.; Salam, A.; Wei, Q. Development of bacterial cellulose nanocomposites: An overview of the synthesis of bacterial cellulose nanocomposites with metallic and metallic-oxide nanoparticles by different methods and techniques for biomedical applications. *J. Ind. Text.* **2022**, *51*, 1886S-1915S.
- [5] Salama, A. Cellulose/calcium phosphate hybrids: New materials for biomedical and environmental applications. *Int. J. Biol. Macromol.* **2019**, *127*, 606-617.
- [6] Hanif, Z.; Khan, Z. A.; Choi, D.; La, M.; Park, S. J. One-pot synthesis of silver nanoparticle deposited cellulose nanocrystals with high colloidal stability for bacterial contaminated water purification. *J. Environ. Chem. Eng.* **2021**, *9*, 105535.
- [7] Pillai, P.; Kakadiya, N.; Timaniya, Z.; Dharaskar, S.; Sillanpaa, M. Removal of arsenic using iron oxide amended with rice husk nanoparticles from aqueous solution. *Mater. Today: Proc.* **2020**, *28*, 830-835.
- [8] Saputera, W. H.; Putrie, A. S.; Esmailpour, A. A.; Sasongko, D.; Suendo, V.; Mukti, R. R. Technology advances in phenol removals: Current progress and future perspectives. *Catalysts* **2021**, *11*, 998.
- [9] Dhali, K.; Ghasemlou, M.; Daver, F.; Cass, P.; Adhikari, B. A review of nanocellulose as a new material towards environmental sustainability. *Sci. Total Environ.* **2021**, *775*, 25.
- [10] Kumar, A.; Negi, Y. S.; Choudhary, V.; Bhardwaj, N. K. Characterization of cellulose nanocrystals produced by acid-hydrolysis from sugarcane bagasse as agro-waste. *J. Mater. Phys. Chem.* **2019**, *2*, 1-8.
- [11] Restrepo, C. V.; Villa, C. C. Synthesis of silver nanoparticles, influence of capping agents, and dependence on size and shape: A review. *Environ. Nanotechnol. Monit. Manag.* **2021**, *15*, 100428.
- [12] Vanderfleet, O. M.; Cranston, E. D. Production routes to tailor the performance of cellulose nanocrystals. *Nat. Rev. Mater.* **2021**, *6*, 124-144.
- [13] Saleem, M. Possibility of utilizing agriculture biomass as a renewable and sustainable future energy source. *Helion.* **2022**, *8*, E08905.
- [14] Fadakar, A.; Montazer, M.; Harifi, T. Mahmoudi, M. R. Innovative preparation of bacterial cellulose/silver nanocomposite hydrogels: In situ green synthesis, characterization, and antibacterial properties. *J. Appl. Polym.*

*Sci.* **2022**, *138*, 49824.

- [15] Ahmad, T.; Guria, C.; Shekhar, S. Effects of inorganic salts in the casting solution on morphology of poly(vinyl chloride)/bentonite ultrafiltration membranes. *Mater. Chem. Phys.* **2022**, *280*, 125805.
- [16] Amiri, M.; Salavati-Niasari, Z. M.; Akbari, A.; Gholami, T. Removal of malachite green (a toxic dye) from water by cobalt ferrite silica magnetic nanocomposite: Herbal and green sol-gel autocombustion synthesis. *Int. J. Hydrogen Energy.* **2017**, *42*, 24846-24860.
- [17] Xu, L.; Wang, Y.-Y.; Huang, J.; Chen, C.-Y.; Wang, Z.-X.; Xie, H. Silver nanoparticles: Synthesis, medical applications and biosafety. *Theranostics.* **2022**, *10*, 8996-9031.
- [18] Chieng, B.; Syn, L.; Nor, I.; Yoon, T.; Yuet, L. Isolation and characterization of cellulose nanocrystals. *Polymers.* **2017**, *9*, 355.
- [19] Siqueira, M. C.; Coelho, G. F.; de Moura, M. R.; Bresolin, J. D.; Hubinger, S. Z.; Marconcini, J. M.; Mattoso, L. H. Evaluation of antimicrobial activity of silver nanoparticles for carboxymethylcellulose film applications in food packaging. *J. Nanosci. Nanotechnol.* **2014**, *14*, 5512-5517.
- [20] Sharma, R. K.; Yadav, S.; Dutta, S.; Kale, H. B.; Warkad, I. R.; Zbořil, R.; Varma, R. S.; Gawande, M. B. Silver nanomaterials: synthesis and (electro/photo) catalytic applications. *Chem. Soc. Rev.* **2021**, *50*, 11293-11380.
- [21] Chieng, B.; Syn, L.; Nor, I.; Yoon, T.; Yuet, L. Isolation and characterization of cellulose nanocrystals from oil palm mesocarp fiber. *Polymers.* **2017**, *9*, 355-366.
- [22] Sahoo, T. R.; Prelot, B. Adsorption processes for the removal of contaminants from wastewater: The perspective role of nanomaterials and nanotechnology. In *Nanomaterials for the Detection and Removal of Wastewater Pollutants*. Elsevier Inc., 2020; pp 161-222.
- [23] Chinthalapudi, N.; Kommaraju, V. V. D.; Kannan, M. K.; Nalluri, C. B.; Varanasi, S. Composites of cellulose nanofibers and silver nanoparticles for malachite green dye removal from water. *Carbohydr. Polym. Technol. Appl.* **2021**, *2*, 100098.
- [24] Cazón, P.; Velazquez, G.; Ramírez, J. A.; Vázquez, M. Polysaccharide-based films and coatings for food packaging: A review. *Food Hydrocoll.* **2017**, *68*, 136-148.
- [25] Mandal, B.; Rameshbabu, A. P.; Soni, S. R.; Ghosh, A.; Dhara, S.; Pal, S. In situ silver nanowire deposited cross-linked carboxymethyl cellulose: A potential transdermal anticancer drug carrier. *ACS Appl. Mater. Interfaces* **2017**, *9*(42), 36583-36595.
- [26] Eisa, W.; Abdelbaset, T.; Mohamed, E.; Mahrous, S. Crosslinked PVA/PVP supported silver nanoparticles: A reusable and efficient heterogeneous catalyst for the 4-Nitrophenol degradation. *J. Inorg. Organomet. Polym.* **2017**, *27*, 1703-1711.
- [27] Heidari, Z.; Pelalak, R.; Malekshah, R. E.; Pishnamazi, M.; Marjani, A.; Sarkar, S. M. Molecular modeling investigation on mechanism of cationic dyes removal from aqueous solutions by mesoporous materials. *J. Mol. Liq.* **2021**, *329*, 115485.
- [28] Pandian, A. M. K.; Karthikeyan, C.; Rajasimman, M. Isotherm and kinetic studies on adsorption of malachite green using chemically synthesized silver nanoparticles. *Nanotechnol. Environ. Eng.* **2017**, *2*, 2.